An analysis of anterior segment development in the chicken eye

Accepted Manuscript

An analysis of anterior segment development in the chicken eye

Violeta Trejo-Reveles, Lynn McTeir, Kim Summers, Joe Rainger

PII:	S0925-4773(17)30816-X
DOI:	doi:10.1016/j.mod.2018.03.001
Reference:	MOD 3492
To appear in:	*Mechanisms of Development*
Received date:	8 December 2017
Revised date:	30 January 2018
Accepted date:	7 March 2018

Please cite this article as: Violeta Trejo-Reveles, Lynn McTeir, Kim Summers, Joe Rainger , An analysis of anterior segment development in the chicken eye. The address for the corresponding author was captured as affiliation for all authors. Please check if appropriate. Mod(2017), doi:10.1016/j.mod.2018.03.001

An analysis of anterior segment development in the chicken eye

Violeta Trejo-Reveles[1,2], Lynn McTeir[1,2], Kim Summers[2,3*] and Joe Rainger[1,2*]

1. The Roslin Institute Chicken Embryology (RICE) Group.

2. The Roslin Institute and Royal Dick School of Veterinary Studies, University of Edinburgh, Easter Bush Campus, Midlothian, EH25 9RG, UK

3. Mater Research Institute-UQ, Translational Research Institute, 37 Kent St, Woolloongabba, Queensland 4102, Australia

*__Authors for correspondence:__

joe.rainger@roslin.ed.ac.uk

Kim.summers@mater.uq.edu.au

Funding:

JR is funded by Fight for Sight (UK) with an Early Career Investigator Fellowship [Grant number1590/1591].

VTR is funded by a CONACYT (Mexico) international studentship

LM is funded by a BBSRC Roslin Institute core institute grant

KS is supported by a BBSRC Roslin Institute core institute grant and by the Mater Foundation, Australia

Key words:

Eye development, anterior segment, glaucoma, chicken embryo

Running title:

Chick anterior segment development

Abstract

Precise anterior segment (AS) development in the vertebrate eye is essential for maintaining ocular health throughout life. Disruptions to genetic programs can lead to severe structural AS disorders at birth, while more subtle AS defects may disrupt the drainage of ocular fluids and cause dysregulation of intraocular pressure homeostasis, leading to progressive vision loss. To date, the mouse has served as the major model to study AS development and pathogenesis. Here we present an accurate histological atlas of chick AS formation throughout eye development, with a focus on the formation of drainage structures. We performed expression analyses for a panel of known AS disorder genes, and showed that chick PAX6 was localized to cells of neural retina and surface ectoderm derived structures, displaying remarkable similarity to the mouse. We provide a comparison to mouse and humans for chick AS developmental sequences and structures and confirm that AS development shares common features in all three species, although the main AS structures in the chick are developed prior to hatching. These features enable the unique experimental advantages inherent to chick embryos, and we therefore propose the chick as an appropriate additional model for AS development and disease.

1. Introduction

The vertebrate eye is a complex sensory organ that acts as an extension of the brain to provide visual detail of an organism's surroundings. It has adapted through evolution to enable different species to see in the dark, under water, over great distances, and across a variable spectrum of light wavelengths[1], reflecting species habitation in diverse ecological niches. Consequentially, although all vertebrates have camera eyes (composed of lens and retina), the precise structure of the eye varies with the requirements of the individual species.

The front of the vertebrate eye, described as the anterior segment (AS), contains transparent structures that collect and focus light (the lens and cornea), and muscular structures that facilitate this (iris and ciliary body). The anterior segment is lubricated throughout the life course by the aqueous humor, a fluid secreted by the ciliary body into the posterior chamber (the space posterior to the iris but anterior to the lens) which then flows through the pupil to the anterior chamber (the space between the iris and cornea). This humor is removed from the eye via outflow through intertrabecular spaces in the trabecular meshwork in the iridocorneal angle (at the recess between the iris-foot and cornea), into Schlemm's canal and from there into the venous system. The balance between secretion and drainage maintains intraocular pressure (IOP) homeostasis, which is essential for the healthy function of the eye[2]. Malformation, injury, or obstruction to tissues in the AS and drainage structures can lead to raised IOP and subsequent damage to the retina and optic nerve, manifesting as glaucoma[3]. Primary open angle glaucoma (POAG), the most common form, is a complex inherited trait defined by increased resistance to drainage through the trabecular meshwork. POAG may affect both humans and companion animals, with a significant burden on health and morbidity[4,5]. Primary angle closure glaucoma (PACG), involves narrowing of the iridocorneal angle through contact

between the iris and trabecular meshwork. It is likely also a complex inherited trait and is more common in people living in Asia[6,7]. A form of narrow or closed angle glaucoma is also seen in dogs, associated with goniodysgenesis, a congenital malformation of the pectinate ligament in the drainage angle[8].

Genome-wide association studies have been highly successful in identifying several POAG-associated loci in humans, and genetic linkage studies have implicated candidate genes within chromosomal regions in POAG affected families[9,10]. In addition, genome-wide studies focused on patients of Asian ancestry have identified a number of loci associated with PACG[7,11]. Yet, the identification of precise causative alleles has been elusive using these approaches. In contrast, DNA sequencing efforts have identified specific single-gene causes for POAG[10], however those variants so far identified only account for less than 10 % of all glaucoma cases. Next generation sequencing technologies (whole exome and complete genome) may yet improve this situation[9]. These are clearly genetically heterogeneous and highly complex diseases, and human genetics approaches are currently limited in their ability to identify their direct causes.

Conditions that affect the structural development of the AS are generally described as anterior segment dysgenesis (ASD) disorders: a heterogeneous group of diseases including aniridia (absence of iris), iris hypoplasia (malformed iris structures), ectopia lentis (subluxation or dislocation of the lens), corneal opacity, congenital cataract, adhesions between the lens and iris or lens and cornea, abnormal drainage angle (including goniodysgenesis), endothelial dystrophia, sclerocornea and megalocornea. Although genetic causes of many ASD have been identified (reviewed in[12]), many cases still lack a genetic diagnosis. Consequently, there remain major gaps in our understanding of the genetic and molecular mechanisms that guide the development of the AS and drainage structures.

Understanding the precise contribution of POAG and PACG candidate genes to development and homeostasis of the AS also requires a thorough understanding of how these structures develop.

Studies of human AS development are limited due to specimen availability, with few reports available illustrating its complete development. The most comprehensive studies have been limited in sample numbers, and biased towards early eye development[13,14], and to date, Ida Mann's robust analysis of human AS development remains the exceptional authoritative reference[15]. To augment these, detailed developmental analyses in mice have been performed[16], and the mouse has proved to be a useful genetic tool for functional analyses of some ASD genes[12,17]. However, mouse anterior segments are small and their eyes are highly compact with a large lens and thick retina; for example see Figure 1 of [18]. The mouse AS also develops over a long time period, ranging through embryonic stages to several weeks after birth. Supportive additional model systems may help improve our understanding of ASD and glaucoma causation, and offer inherent and unique advantages over existing mouse models.

Chicken embryos are an excellent model for the study of vertebrate development and are particularly useful for the study of eye diseases[20], retinal development[21], developmental gene expression, patterning and morphogenesis[22,23], and cell-fate mapping[24]. However, to our knowledge the histological sequence of chick AS development has not been clearly described. In the present study, we explored the anatomy and structural development of the chick AS - with focus on the drainage structures - to provide an assessment of its suitability as a model for future in-depth studies.

2. Methods

2.1 Chick embryos

Fertile eggs (wild-type Hy-Line Brown layers) were obtained from The National Avian Research Facility (Roslin Institute) and incubated at 37°C until they reached the desired stage, using Hamburger Hamilton (HH) staging [25] as a guide. A minimum of three eyes from independent chicks were used for each stage analyzed.

2.2 Histological staining

Enucleated eyes were fixed in 4 % paraformaldehyde (PFA) for 12-24 h on a roller shaker at 4°C, and then quickly rinsed in PBS before they were dehydrated in an ethanol-PBS series of 30 %, 50 %, 70 % and 100 % (1 hour each at room temperature). Samples were paraffin-embedded in a Leica ASP200 tissue processor. Once in paraffin, eyes were cut manually in the sagittal plane using a microtome setting the thickness between 8-10 µm. All slides were stained using a Leica Autostainer XL with a conventional H&E program. All histological data was captured with a Hamamatsu Slide Scanner using a 40x air objective, and analyzed using NPD View.2 Software (Hamamatsu).

2.3 Gene expression analysis

Expression of known ASD genes was analyzed in the developing chick using reverse transcriptase PCR (RT-PCR). We dissected anterior segments from chicks at embryonic days (E) 9, 12, 14 and three days post-hatch (P3). For E7 embryos we used whole eyes. For each stage, we used a minimum of six eyes from different chicks. Samples were pooled and RNA was extracted using

TriZol Reagent (Thermo Scientific) according to the manufacturer's published protocol. We performed cDNA synthesis using 2.0 µg total RNA input with Superscript III reverse transcriptase (Thermo Scientific) with random hexamers and following the manufacturer's instructions to a total reaction volume of 20 µl (negative controls were performed with no reverse polymerase added). For RT-PCR reactions, oligonucleotide primers were designed using Primer3 (http://bioinfo.ut.ee/primer3-0.4.0/) using transcript data obtained from Ensembl (Gallus_gallus-5.0; http://www.ensembl.org/Gallus_gallus/Info/Index). All primers were designed to amplify across multiple introns, except for the single-exon genes *FOXC1* and *FOXE3*. RT-PCR reactions were performed in 25 µl volumes containing final concentrations of: 0.2 µM primers, 0.2 µl Faststart Taq Polymerase (5 U/µl; Roche), 1X PCR reaction buffer (2 mM MgCl2), 200 µM of each dNTPs and 1.0 µl input cDNA. Cycle conditions were: 95^{o}C for 4 mins; then 35 cycles of 95^{o}C for 45 s, 56^{o}C for 45 s, 72^{o}C for 1 min; then 72^{o}C for 10 mins. Amplicons were run on 1 % agarose gels with 0.5 % TBE running buffer. A list of specific oligonucleotide primers is provided in the Key Resources Table.

2.4 Mouse gene expression analysis

A developmental time course of mouse eyeball from C57BL/6J mice of mixed sexes was available through the FANTOM5 project[26–28]. Gene expression levels, based on cap analysis of gene expression (CAGE), which quantifies expression based on detection of the initial 27 nucleotides of transcripts, were estimated using the Zenbu browser (http://fantom.gsc.riken.jp/zenbu/) by recording the total tags per million across the whole gene region. Accession numbers were E15.CNhs10593.426-16C9, E17.CNhs11023.1261-18D4, N02.CNhs11205.1551-44G8, N16.CNhs11188.777-19A2, adult.CNhs10484.31-12G4. Expression profiles of individual genes

mentioned can be viewed on the Zenbu browser by entering the gene name in the search box. Data is supplied in **Supporting Table S1**.

2.5 Immunofluorescence analysis for PAX6

Wild type fertilized eggs were collected and incubated for the required days (E9 & E11) at 37^{o}C. Eyes were resected and the entire anterior region was dissected and fixed in 4 % PFA for 2 hours at room temperature. Samples were then rinsed once in PBS and then immersed in 15 % sucrose-PBS solution on a rotating shaker overnight at 4^{o}C. Samples were then equilibrated in 7 % gelatin:15 % sucrose-PBS for 4h in a waterbath at 37^{o}C before cooling and embedding in blocks. Sections were cut at 10 µm, mounted on Superfrost plus (Thermo-Fisher) slides and air-dried for 1 hour at room temperature. Sections were then frozen at -20^{o}C until required. For immunofluorescence, sections were thawed and rinsed twice in PBS (for 5 minutes each), then blocked with 1 % BSA in a 0.25 % Triton-X-100 PBS solution. Monoclonal antibodies raised against a highly conserved region of human PAX6 (a kind gift from Professor David FitzPatrick, at the MRC Human Genetics Unit) were used at a dilution of 1:20 in 0.1 % BSA in a 0.25 % Triton-X-100 PBS solution overnight at 4^{o}C. Slides were then rinsed 5 times in PBS and were then incubated in 1:1000 diluted Goat anti-Mouse IgG (H+L) Cross-Adsorbed antibody (Alexa Fluor 594 nm; Thermo-Fisher Product #A-11005) with Phalloidin Control Dylight 488 (Thermo-Fisher. Cat no.21833) diluted at 1:500 for 1 hour at room temperature. Slides were then rinsed 5 times in PBS and mounted with Prolong Gold Antifade with DAPI (Thermo-Fisher. Cat no.P36941). Images were captured using a Nikon C1 confocal microscope and a Plan Apochromat 60.0x/1.40/0.13 Oil objective and images were processed using FIJI open source software[29].

3. Results

3.1 Embryonic development

We began our analysis at chick embryonic day (E)7, corresponding to stages 31-33 [25], before any signs of anterior segment development at the histological level in the eye (**Figure 1a**). The future iris and ciliary body had not become apparent within the ciliary margin, which at this stage was an undifferentiated extension of neural retina and retinal pigmented epithelium. The anterior chamber - defined by the limits of cornea, iris and lens – was apparent by E9 with an acute iridiocorneal angle (**Figure 1b**). Here, the lens had detached from the cornea and the iridocorneal angle marked the junction between corneal endothelium and iris stroma, forming the anterior chamber. The iris had extended towards the lens and the ciliary processes had begun to fold, with pigmented and non-pigmented epithelia clearly evident. The corneal stroma showed some stratification. Posterior to the iridocorneal angle, the future trabecular meshwork (TM) anlage was composed of a compressed and undifferentiated mass of mesenchymal cells, bordered by cells extending from the corneal stroma. No drainage structures were visible at this stage.

The iridiocorneal angle had become less acute by E11 and the TM had expanded (**Figure 1c**), forming the first intertrabecular spaces within the drainage angle. Blood vessels of the presumptive scleral venous sinus group had become evident in the intrascleral region of the angle, with red blood cells clearly visible. The posterior margins of the iris had developed pigment and the anterior edge of the ciliary body had become distinct from the TM.

By E14 the corneal endothelium was physically distinct from the iris foot (**Figure 1d**), separated by an extension of cells between the two structures to form a perpendicular recess in the developing angle. The TM cells were becoming sparsely arranged with large intertrabecular spaces

forming between them. At their anterior limit, these long processes were compact and continuous, and formed a junction between the TM and the anterior chamber, and resembled the fibers of the pectinate ligament (PL) seen in other species [30]. Scleral ossicles (SO) were visible adjacent to the scleral-corneal junction, and development of the anterior ciliary muscles was observable posterior to the SO. Several more intrascleral blood vessels were now visible anterior to the TM. At E16, the most significant changes observed were lengthening of the PL, with the result that the iris and cornea were further apart (**Figure 1e**). There was an additional reduction of cells within the TM, and well defined boundaries had arisen between TM, the developing anterior ciliary musculature, and the ciliary epithelium. The first definitive signs of Schlemm's canal development were evident at E19 (**Figure 1f**), accompanied by an almost complete absence of cells in the TM, distinct widening of the iridiocorneal angle, maturation of SO, lengthening of the iris, and further development of the anterior ciliary muscles.

3.2 Post-hatch development

In early post-hatch (P3) chick eyes the AS and drainage structures appeared completely mature (**Figure 2a-c**). Schlemm's canal had lengthened and widened, and had matured with an asymmetrical structure: tightly-organized endothelial cells bordered the lumen at the anterior aspect, and several layers of TM cells formed a loosely arranged border at the posterior aspect (**Figure 2b**). Schlemm's canal was immediately adjacent to the intrascleral blood vessels and anterior ciliary muscles. At P10 (**Figure 2c**) the angle was fully mature with the TM clearly visible as a composition of loosely arranged cells at the posterior margin of Schlemm's canal. There were extending trabecular beams from the anterior-posterior region (terminating at the corneal epithelium) towards the ciliary

body and iris, and some complete trabecular bands that appeared to fully cover the entry to the recessed angle.

3.3 Comparative analysis between mouse, human and chick AS development.

We compared our staging data for chick AS development to the equivalent AS structure development in the mouse (**Table 1**). Overall, observable chick eye development (from optic vesicle outgrowth to drainage angle maturation) took approximately 22 days and was structurally complete at hatching. In mouse, the equivalent developmental process occurred over more than 33 days, with drainage angle maturation not complete until after weaning[16]. The appearance of presumptive TM mesenchyme occurred at E9 in chick, requiring a further <14 days to mature. In the mouse the dense packing of cells in the TM anlage appears around P2 and does not complete until at least P21. Similarly, Schlemm's canal structures in the chick were present from E19 onwards and were fully mature by P3; in mouse these foci are not evident until P10 and are not structurally mature until P14.

Comparison with human AS development after the 8th gestational week is limited to histological data presented in two studies[13,15]. However, these reports show the human eye develops an anterior chamber between the 15th - 17th week, and presumptive TM condensations at the sclerocorneal region are evident from as early as the 15th week. The appearance of intercellular spaces and changes to the morphology of cells within this region is visible in week 22 embryos. Structures consistent with the development of Schlemm's canal have also emerged at this stage. Although the subsequent sequences of maturation for these structures remains unclear in humans, there are numerous examples of sections of the angle in the adult eye that are available in the public domain. Importantly, these show clearly that the human angle is deep and wide, similar to chick. Schlemm's canal in all three species is similarly located at the posterior base of the corneal

endothelium. However, in the chick, beams from the TM extend from Schlemm's canal to reach the posterior of the ciliary body. In contrast, the TM of mouse and human are located immediately in contact with Schlemm's canal and are more tightly aggregated.

Developmental event	**Chick**	**Mouse**	**Human**
Optic vesicle outgrowth	E2	E9	4-5W
Lens pit	E2.5	E9.5	5W
Optic cup	E3	E10.5	5-6W
Optic fissure closure	E8	E12	6-7W
Iris stroma lengthening	E9	E15-16	15W
Anterior chamber formation	E9	E15.5	15-17W
Ciliary body folding	E9	E18.5	22W
TM anlage mesenchyme	E9	P2	15-17W
Inter-TM spaces	E11	P10	22W
Focal appearance of SC	E16	P10	22W
Deep angle present	E16	P14	7M
Final maturation of drainage angle	E18-P3	P21+	*7M+

Table 1. Comparison between chick and mouse for key events during anterior eye development. Chick data was derived from the present study; mouse and human data was from[13–17]. Shaded regions correspond to post-hatch and post-natal periods of eye development. Abbreviations: E, embryonic day; P, post-natal/hatch; W, weeks; M, months. *The timing of final drainage angle maturation in humans has not been accurately described.

3.4 ASD gene expression in chick.

We then asked whether chick homologues of known human anterior segment dysgenesis genes were expressed during development of the chick AS. We extracted RNA from whole eye tissue at E7 (pre-angle formation) and for days 9, 12, 14 and Post hatch day 3 we dissected the developing iridiocorneal angle (e.g. to include the developing TM, anterior iris, ciliary body and cornea, and all other tissues in this region). We performed semi-quantitative RT-PCR on our panel of genes and observed strong and constant expression of *PITX2*, *FOXC1*, and *PAX6*; and biphasic expression of *CYP1B1* and *FOXE3* (**Figure 3a**). *ITPR1* appeared to show a slight increase in expression from E9 to subsequent stages E12, E14 and P3.

We also extracted quantitative gene expression for this panel using data for whole mouse eyes during corresponding stages of AS development (**Figure 3b**), from a public resource provided by the FANTOM5 project. *Pax6* was the highest expressed of these genes, and levels remained relatively constant. In contrast to chick, we observed a graded reduction of *Pitx2* and *FoxC1* expression from initially high expression levels at E15. For *Cyp1b1*, expression peaked at P2 and then displayed a marked subsequent reduction. Both *Foxe3* and *Itpr1* displayed dynamic expression patterns at these time points. *Foxe3* and *Cyp1b1* were the lowest expressed of these genes in mouse, which corresponded with our observations in chick.

PAX6 is a major locus for both human and mouse ASD and POAG[12,31], was the highest expressed gene observed in the mouse ASD panel, and was expressed at all stages analyzed in the chick angle. We therefore chose to establish the localization of PAX6 protein in the developing chick anterior segment, when the structural development of this region was first apparent. We observed PAX6 positive nuclei in the ciliary body, some distinct cells in the anterior iris stroma, in the lens epithelium, corneal epithelium, and in the ganglion and neuroblastic cells of the maturing neural

retina of E9 eyes (**Figure 3c**), and at in the same locations at E11 (not shown). We did not observe PAX6-positive cells in the corneal stroma or endothelium at either stages. Using fluorescent-conjugated phalloidin to as a counterstain to highlight cell boundaries and mark F-actin localization in the chick eye, we revealed that the developing trabecular mesenchyme was a region rich in Filamentous actin, but was devoid of any nuclear PAX6. Cells positive for PAX6 in the iris were at the most anterior regions and localized to areas of the developing sphincter muscles, yet the remaining iris stroma was absent for PAX6. The ciliary body displayed an apparent gradient of PAX6 signal, increasing anteriorally and the strongest signal in ciliary epithelial cells most immediately adjacent to the lens.

4. Discussion

The chick eye makes up a considerable proportion of the embryo for much of the time from laying to hatch (for example see the images in Hamburger and Hamilton[25]) and both the embryonic and adult eye is larger than many other model organisms. Chicken eyes are similar in structural proportion to humans, with a thin retina, flattened lens and large vitreous volume. The chick is also highly accessible during development, and many experimental manipulations are possible. Despite these advantages, use of chick as a model for eye development declined in popular use due to the emergence of powerful genetic tools in both mouse and zebrafish (e.g. gene knock-outs and reporter-lines; morpholinos). In particular, the mouse has been the predominant model organism for assessing AS development and POAG pathogenesis[16,17]. The chicken genome was first published in 2004[32] and is now comprehensively annotated, publically-available, and supported by multiple tissue-specific transcriptomic datasets. Consequently, genetic tools are rapidly emerging for the specific study of gene-function *in ovo*, including tissue-specific gene editing[33–35], multiple fluorescent reporter lines[36],

and the ability to deliver genetic material specifically into the developing chick eye[37–40]. As a result, the chick is now becoming more widely used for studies of eye development[21] and these advances provide novel opportunities for more in-depth molecular and genetic interrogation of multiple aspects of eye development[20,21].

Given these experimental advantages, we were keen to establish whether the chick may provide an additional model for further studies of AS development and disease. To our knowledge, no prior comparison of AS developmental staging had been performed between chick, humans and mice. Notably, all the structures in the human drainage angle develop during embryological or fetal stages, which is more consistent with our data for the sequence of chick angle formation than for mouse. Chicks hatch with their eyes open, and can forage for food almost immediately. To support this, development of a functional visual system is largely complete within their gestational (pre-hatch) period. In contrast, mice are born with their eyes closed and they do not open until weaning stages (approximately three weeks). Only then do pups begin to learn feed independently. These features correspond to the lengthy developmental sequence observed in mice, but contrast with the situation in humans, where the drainage angle at 7 months of fetal development is highly comparable to those in adults [15]. Thus, human and chick AS and drainage angle formation correlate well in their developmental sequences.

The major structural differences between the mature chick and human angle is at the TM. We showed that in the chick eye, the TM consisted of loosely arranged layers of cells immediately overlying Schlemm's canal, but also comprised trabecular beams (and large intercellular spaces) that extended from the anterior margin of the canal to the ciliary body foot and iris foot in the angle recess. In addition, there were some complete trabecular bands at the entry to the recessed angle, emanating from the point where the corneal endothelium and TM met. These structurally

corresponded to the pectinate ligament observed in other species[41,42], but are not observed in the human angle. Nevertheless, the development of these structures in chick appeared to emanate from the condensed collection of cells at the early sclerocorneal region that has been observed in all three species. The chick will provide an excellent model to understand the genetic and molecular programs required for these cells to develop into the TM and additional processes.

To be a suitable model for human AS development the chick eye must also support analyses of the gene networks governing this process, and therefore the orthologues of human AS genes should be expressed in the developing chick eye. We specifically dissected the chick iridiocorneal region during key stages of its development, and then performed semi-quantitative gene expression assays for a panel of the main ASD-causing or glaucoma risk associated genes: *PAX6*, *PITX2*, *FOXE3*, *FOXC1*, *ITPR1* and *CYP1B1* [12,43]. We observed that in chick, these genes were all strongly and consistently expressed in the angle (except for *CYP1B1*, whose expression was low and appeared undetectable at E9), indicating a functional requirement and a prediction that they will have similar developmental roles to their human orthologues. This knowledge supports further exploration of their roles using the chick embryo.

As a similar dissection-based approach is difficult in the mouse angle, we made use of publically available transcriptome data for the whole mouse eyeball to compare expression of these orthologues in mouse during development. *Pax6* was consistently the highest expressed gene, and reflecting its multiple roles during development of wide range of ocular tissues (neural retina, iris and ciliary body, corneal epithelium and lens). In contrast, expression of both *Pitx2* and *Foxc1* was highly dynamic: highest at E15.5 (initial AS chamber formation) and then dramatically reduced. This is likely to be due to the sequential refinement of their expression to developing AS structures, and the limit of resolution for this whole-eye data. For example, both *Pitx2* and *Foxc1* are first expressed

throughout the periocular mesenchyme surrounding the early mouse eye, but then later become restricted to the developing TM at E16.5-E18.5[44–46]. In contrast, we showed that all three of these genes were highly constitutively expressed throughout chick angle development. Of interest, *Itpr1*, *Foxe3* and *Cyp1b1* all showed apparently dynamic expression in the mouse eye, but there is limited available data relating to their precise distribution during AS development. Our data showed these three genes were all transcribed within the chick angle, with some evidence for dynamic expression. This should be followed up with staged in situ hybridization to pinpoint exact expression domains, but also supports the potential for chick precise dissections of the iridiocorneal angle coupled with whole transcriptomics, to identify important genetic pathways in an unbiased approach. Our immunostaining for chick PAX6 protein localization corresponded well with known Pax6 localization domains in the mouse, with positive nuclei observed in the surface ectoderm derivative tissues of the corneal and lens epithelia, and in the neural retina derived ciliary body epithelium, and in the neuroblastic cells within the central neural retina. We also observed small populations of PAX6 positive cells in the anterior iris stroma, localized to cells of the iridial muscle sphincter. However, we were unable to detect nuclear PAX6 in cells of the developing trabecular meshwork, the iris stroma, corneal endothelium or in the corneal mesenchyme - cells that originate from neural crest cells in the mouse eye[47]. In combination, our data suggest that conserved genetic mechanisms for AS development occur in human, mouse and chick; but that the chick eye provides a unique advantage for identifying a genetic requirement for human ASD candidates prior to undertaking mechanistic and deeper developmental studies.

To our knowledge, this study provides the first clear and accessible histological atlas of chicken anterior segment development, with an emphasis on structures within the drainage angle. We highlight the developmental timings of iridiocorneal angle, trabecular meshwork, Schlemm's canal,

ciliary muscles and intrascleral vessel formation. We show that these structures develop between gestational days 9-19, and fully mature immediately after hatching. The chick iridiocorneal angle was easy to dissect and expression of known human ASD and POAG genes was consistent with an evolutionarily conserved role in chick AS development. In combination with its experimental accessibility and versatility, and the emergence of multiple novel techniques for *in ovo* studies; we therefore propose the chick to be a valuable model to perform molecular and genetic studies of AS development and disease mechanisms.

5. Figure legends

Figure 1. Anterior segment development begins during mid-embryonic stages.

Histological analyses (H&E) of representative chick eyes between E7 and E19 show the development of the anterior segment and drainage angle. (**a**) At E7 the anterior eye is composed of cornea (C), lens (L) and the distal optic cup composed of neural retina (NR) and retinal pigmented epithelium (RPE). The ciliary margin (CM) is histologically indistinct from the neural retina at this stage. The margin of the optic cup is parallel to the equator of the lens (arrow). (**b**) At E9 the iridiocorneal angle (IA) separates the iris stroma (IR) from the cornea, forming the anterior chamber (AC). A thickening of cells adjacent to this region marks the boundary of the developing drainage angle (arrowheads), and is anterior to the location of the future trabecular meshwork (arrow). At this stage, the iris has extended towards the lens and folding of the ciliary body (CB) has initiated, with pigmented and non-pigmented epithelia evident (PE and NPE, respectively). (**c**) At E11 the developing trabecular meshwork (TM) has become less tightly packed creating large intertrabecular spaces. The first intrascleral vessel is visible as a small vacuole at the posterior limit of the cornea (arrowhead). The iridiocorneal angle has increased, and the iris and the epithelia of the ciliary body have begun to separate from the TM (asterisks). Fibers connecting the lens to ciliary body are evident (arrows). (**d**) The trabecular meshwork within the angle has expanded considerably at E14, with large open intertrabecular spaces now present. Complete separation of the iris and cornea has occurred at the iridiocorneal angle, leaving the immature pectinate ligament connecting the iris foot (IF) to the cornea. Sphincter muscles (SM) have differentiated at the distal iris and anterior ciliary muscles (arrows) have formed anterior to the immature TM. Multiple intrascleral vessels (black arrowheads) and scleral ossicles (SO) (white arrowhead) are now visible. (**e**) In the E16 eye, the trabecular meshwork has widened in area but is now largely devoid of populating cells. It is bordered at its

posterior edge by the limit of the developing ciliary body epithelia (black dashed line) and anteriorly by the limit of the immature presumptive Schlemm's canal (SC) region (blue dashed line). The PL have lengthened to accommodate the increased axial distance between the corneal epithelium and iris. (**f**) The maturing scleral ossicles are now clearly visible at the scleral-corneal boundary, and anterior ciliary muscles are more easily defined (arrows). The developing Schlemm's canal is visible as gaps within the mesenchymal tissue anterior to the TM (arrowheads). The iris has thinned and extended further towards the lens and there is a recessed pit at the corneal epithelium where the pectinate ligament fibers attach (asterisk). SF – spaces of Fontana; ICM – intermediate ciliary muscle. Red lines indicate the iridiocorneal angles in **b** & **c**, and red asterisks mark tissue-processing artefacts. Scale bars = 100 μm.

Figure 2. Anterior segment maturation in the post-hatch chick.

Histological analyses (H&E) of representative chick eyes at post-hatch day 3 and 10 (***a***) Development of the drainage region appears mature at post-hatch day 3. Spaces of Fontana (SF) are present between the trabecular beams in the wide-open drainage chamber. (***b***) Enlarged view of ***a*** shows the arrangement of cells within the Schlemm's canal and the intrascleral vessels at the anterior aspect (arrows) and posterior aspect (arrowheads) of Schlemm's canal. (***c***) Complete maturation of the AS and drainage angle in the P10 chick eye. S – Sclera; SO – scleral ossicles; ACM – anterior ciliary muscle; ISV –intrascleral vessels, ICM – intermediate ciliary muscle. Scale bar = 100 μm

Figure 3. ASD gene expression dynamics during the chick and mouse AS development sequence. (***a***) RT-PCR analysis of dissected iridiocorneal angle of the chick through key developmental stages for anterior segment dysgenesis and POAG associated genes. (***b***) Equivalent analysis of gene expression data in whole mouse eyes obtained from FANTOM5 (http://fantom.gsc.riken.jp/zenbu/). Light grey – embryonic stages; dark grey – neonatal stages; black

– adult. (***c***) Immunofluorescence analysis of PAX6 localisation (magenta) and filamentous actin (phalloidin, green) in the developing chick anterior segment in regions of the developing (i) cornea, (ii) trabecular meshwork, (iii) iris, and (iv) neural retina. PAX6 nuclei positivity was observed in the ciliary body (ii & iii; arrowheads) in the anterior iris (yellow arrows in iii) and lens epithelium (white arrows in iii). The iridiocorneal angle recess is marked by red hatching (in panels i & ii). Abbreviations: CS, corneal stroma; CE, corneal epithelium; TM, trabecular meshwork anlage (large white hatching); IR, iris; CB, ciliary body; PE, pigmented epithelium of ciliary body; NPE, non-pigmented epithelium of ciliary body; LE, lens epithelium; GCL, ganglion cell layer; OS, outer segment; NBL, neuroblastic layer of retina; RPE, retinal pigmented epithelium. Scale bar = 50 µm.

6. Acknowledgments.

We are extremely grateful to staff at the NARF, especially those in the Greenwood building, for flock maintenance and egg supply. We are also grateful to Dr Megan Davey and her lab members for scientific support and the sharing of lab space, resources and expertise.

7. References

1. Nilsson, D. Eye evolution and its functional basis. *Vis. Neurosci.* **30,** 5–20 (2013).
2. Fautsch, M. P. *et al.* Aqueous humor outflow: What do we know? Where will it lead us? in *Investigative Ophthalmology and Visual Science* **47,** 4181–4187 (2006).
3. Weinreb, R. N., Aung, T. & Medeiros, F. A. The pathophysiology and treatment of glaucoma: a review. *JAMA* **311,** 1901–11 (2014).
4. Foster, P. J. The epidemiology of primary angle closure and associated glaucomatous optic neuropathy. *Semin. Ophthalmol.* **17,** 50–58 (2002).
5. Kanemaki, N. *et al.* Dogs and humans share a common susceptibility gene SRBD1 for glaucoma risk. *PLoS One* **8,** e74372 (2013).
6. Quigley, H. A. & Broman, A. T. The number of people with glaucoma worldwide in 2010 and 2020. *Br. J. Ophthalmol.* **90,** 262–7 (2006).
7. Vithana, E. N. *et al.* Genome-wide association analyses identify three new susceptibility loci for primary angle closure glaucoma. *Nat. Genet.* **44,** 1142–1146 (2012).
8. Mellersh, C. S. The genetics of eye disorders in the dog. *Canine Genet. Epidemiol.* **1,** 3 (2014).
9. Liu, Y. & Allingham, R. R. Major review: Molecular genetics of primary open-angle glaucoma. *Exp. Eye Res.* **160,** 62–84 (2017).
10. Allingham, R. R., Liu, Y. & Rhee, D. J. The genetics of primary open-angle glaucoma: A review. *Exp. Eye Res.* **88,** 837–844 (2009).
11. Wiggs, J. L. & Pasquale, L. R. Genetics of glaucoma. *Human Molecular Genetics* **26,** R21–R27 (2017).
12. Sowden, J. C. Molecular and developmental mechanisms of anterior segment dysgenesis. *Eye*

(Lond). **21,** 1310–1318 (2007).

13. McMenamin, P. G. Human fetal iridocorneal angle: a light and scanning electron microscopic study. *Br. J. Ophthalmol.* **73,** 871–9 (1989).
14. O'Rahilly R. The early development of the eye in staged human embryos. *Carnegie instn Wash Publ* **625,** 1–42 (1966).
15. Ida Mann. *The Development of the human eye*. (British Medical Association, 1969).
16. Smith, R. S., Zabaleta, A., Savinova, O. V & John, S. W. The mouse anterior chamber angle and trabecular meshwork develop without cell death. *BMC Dev. Biol.* **1,** 3 (2001).
17. Cvekl, A. & Tamm, E. R. Anterior eye development and ocular mesenchyme: new insights from mouse models and human diseases. *Bioessays* **26,** 374–86 (2004).
18. Tkatchenko, T. V., Shen, Y. & Tkatchenko, A. V. Analysis of postnatal eye development in the mouse with high-resolution small animal magnetic resonance imaging. *Investig. Ophthalmol. Vis. Sci.* **51,** 21–27 (2010).
19. Hitchcock, P. F. Eye, Retina, and Visual System of the Mouse. *J. Neuro-Ophthalmology* **29,** 257–258 (2009).
20. Hocking, P. THE CHICK AS AN ANIMAL MODEL OF EYE DISEASE. *Drug Discov. Today Dis. Model.* (2012).
21. Vergara, M. N. & Canto-Soler, M. V. Rediscovering the chick embryo as a model to study retinal development. *Neural Dev.* **7,** 22–40 (2012).
22. Peters, M. a & Cepko, C. L. The dorsal-ventral axis of the neural retina is divided into multiple domains of restricted gene expression which exhibit features of lineage compartments. *Dev. Biol.* **251,** 59–73 (2002).
23. Schook, P. Morphogenetic movements during the early development of the chick eye. A light

microscopic and spatial reconstructive study. *Acta Morphol. Neerl. Scand.* **18,** 1–30 (1980).

24. Johnston, M. C., Noden, D. M., Hazelton, R. D., Coulombre, J. L. & Coulombre, A. J. Origins of avian ocular and periocular tissues. *Exp. Eye Res.* **29,** 27–43 (1979).

25. Hamburger, V. & Hamilton, H. L. A series of normal stages in the development of the chick embryo. 1951. *Dev. Dyn.* **195,** 231–272 (1992).

26. Kawai, J. *et al.* Functional annotation of a full-length mouse cDNA collection. *Nature* **409,** 685–689 (2001).

27. Forrest, A. R. R. *et al.* A promoter-level mammalian expression atlas. *Nature* **507,** 462–470 (2014).

28. Okazaki, Y. *et al.* Analysis of the mouse transcriptome based on functional annotation of 60,770 full-length cDNAs. *Nature* **420,** 563–573 (2002).

29. Schindelin, J. *et al.* Fiji: An open-source platform for biological-image analysis. *Nature Methods* **9,** 676–682 (2012).

30. Pizzirani, S. & Gong, H. Functional Anatomy of the Outflow Facilities. *Veterinary Clinics of North America - Small Animal Practice* **45,** 1101–1126 (2015).

31. Kroeber, M. *et al.* Reduced expression of Pax6 in lens and cornea of mutant mice leads to failure of chamber angle development and juvenile glaucoma. *Hum. Mol. Genet.* **19,** 3332–3342 (2010).

32. Hillier, L. W. *et al.* Sequencing and comparative analysis of the chicken genome provide unique perspectives on vertebrate evolution. *Nature* **432,** 695–716 (2004).

33. Woodcock, M. E., Idoko-Akoh, A. & McGrew, M. J. Gene editing in birds takes flight. *Mamm. Genome* **28,** 1–9 (2017).

34. Véron, N., Qu, Z., Kipen, P. A. S., Hirst, C. E. & Marcelle, C. CRISPR mediated somatic cell

genome engineering in the chicken. *Dev. Biol.* **407,** 68–74 (2015).

35. Dad Abu-Bonsrah, K., Zhang, D. & Newgreen, D. F. CRISPR/Cas9 targets chicken embryonic somatic cells in vitro and in vivo and generates phenotypic abnormalities. *Sci. Rep.* 1–10 (2016). doi:10.1038/srep34524

36. Davey, Megan G. Balic, Adam. Rainger, Joe. Sang, Helen M. McGrew, M. J. Illuminating the chicken model through genetic modification. *Int. J. Dev. Biol.* (2018).

37. Luz-Madrigal, A., Grajales-Esquivel, E. & Del Rio-Tsonis, K. Electroporation of Embryonic Chick Eyes. *Bio-protocol* **5,** 1–19 (2015).

38. Thangaraj, G., Greif, A. & Layer, P. G. Simple explant culture of the embryonic chicken retina with long-term preservation of photoreceptors. *Exp. Eye Res.* **93,** 556–564 (2011).

39. Shirazi Fard, S., Blixt, M. & Hallböök, F. Whole Retinal Explants from Chicken Embryos for Electroporation and Chemical Reagent Treatments. *J. Vis. Exp.* 1–7 (2015). doi:10.3791/53202

40. Chen, Y.-X., Krull, C. E. & Reneker, L. W. Targeted gene expression in the chicken eye by in ovo electroporation. *Mol. Vis.* **10,** 874–83 (2004).

41. Morrison, J. C. & Van Buskirk, E. M. The canine eye: Pectinate ligaments and aqueous outflow resistance. *Investig. Ophthalmol. Vis. Sci.* **23,** 726–732 (1982).

42. McMenamin, P. G. & Steptoe, R. J. Normal anatomy of the aqueous humour outflow system in the domestic pig eye. *J. Anat.* **178,** 65–77 (1991).

43. McEntagart, M. *et al.* A Restricted Repertoire of De Novo Mutations in ITPR1 Cause Gillespie Syndrome with Evidence for Dominant-Negative Effect. *American Journal of Human Genetics* (2015). doi:10.1016/j.ajhg.2016.03.018

44. Kidson, S. H., Kume, T., Deng, K., Winfrey, V. & Hogan, B. L. M. The Forkhead/Winged-Helix Gene, Mf1, Is Necessary for the Normal Development of the Cornea and Formation of

the Anterior Chamber in the Mouse Eye. *Dev. Biol.* **211,** 306–322 (1999).

45. Acharya, M., Lingenfelter, D. J., Huang, L., Gage, P. J. & Walter, M. A. Human PRKC apoptosis WT1 regulator is a novel PITX2-interacting protein that regulates PITX2 transcriptional activity in ocular cells. *J. Biol. Chem.* **284,** 34829–34838 (2009).

46. Lu, M. F., Pressman, C., Dyer, R., Johnson, R. L. & Martin, J. F. Function of rieger syndrome gene in left-right asymmetry and craniofacial development. *Nature* **401,** 276–278 (1999).

47. Kanakubo, S. *et al.* Abnormal migration and distribution of neural crest cells in Pax6 heterozygous mutant eye, a model for human eye diseases. *Genes to Cells* **11,** 919–933 (2006).

Highlights:

- The chick is an excellent model for developmental biology, in particular due to its resurgent experimental and genetic utilities, and its inherent experimental advantages.
- Here, we establish the chick as an additional model for developmental eye research, focusing on the structural development at the anterior segment (AS) and the ocular drainage structures, orthologous gene expression and localization of PAX6.
- We found common overlaps between chick, mouse and human development. In chick, these processes occur prior to hatching, whereas in mice these events continue to occur long after birth. The chick closely aligned to human AS development, and now permits a broad range of experimental manipulations for ongoing research.
- We propose the chick to be an excellent model system for elucidating disorders affecting the anterior segment, e.g. anterior segment dysgeneses and primary open angle glaucoma.

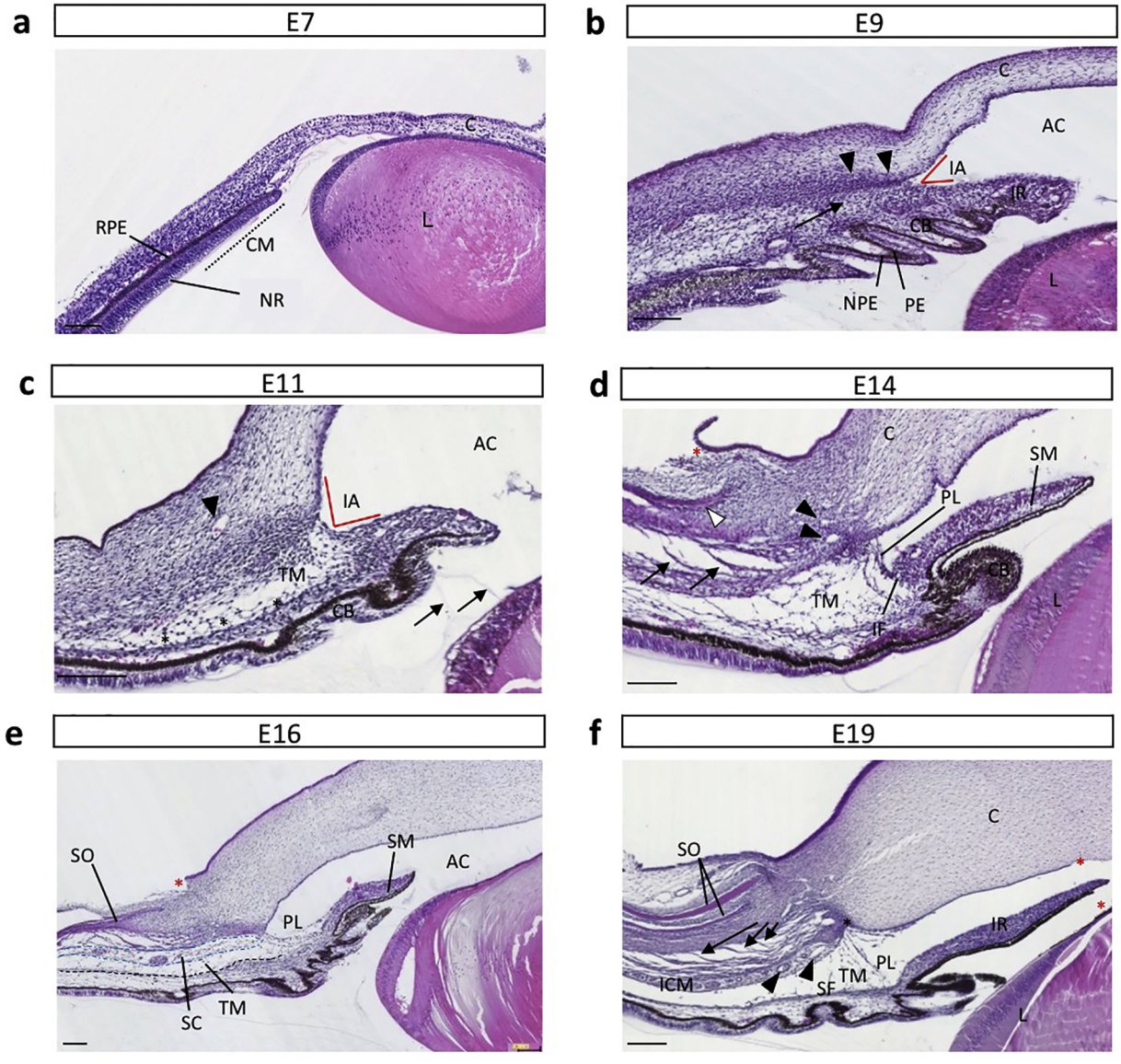
a
E7
C
RPE
CM
L
NR
b
E9
C
AC
IA
IR
CB
NPE
PE
L
c
E11
AC
IA
TM
CB
d
E14
C
SM
PL
CB
TM
IF
L
e
E16
SO
SM
AC
PL
TM
SC
f
E19
C
SO
IR
PL
TM
ICM
SF
L

Figure 1

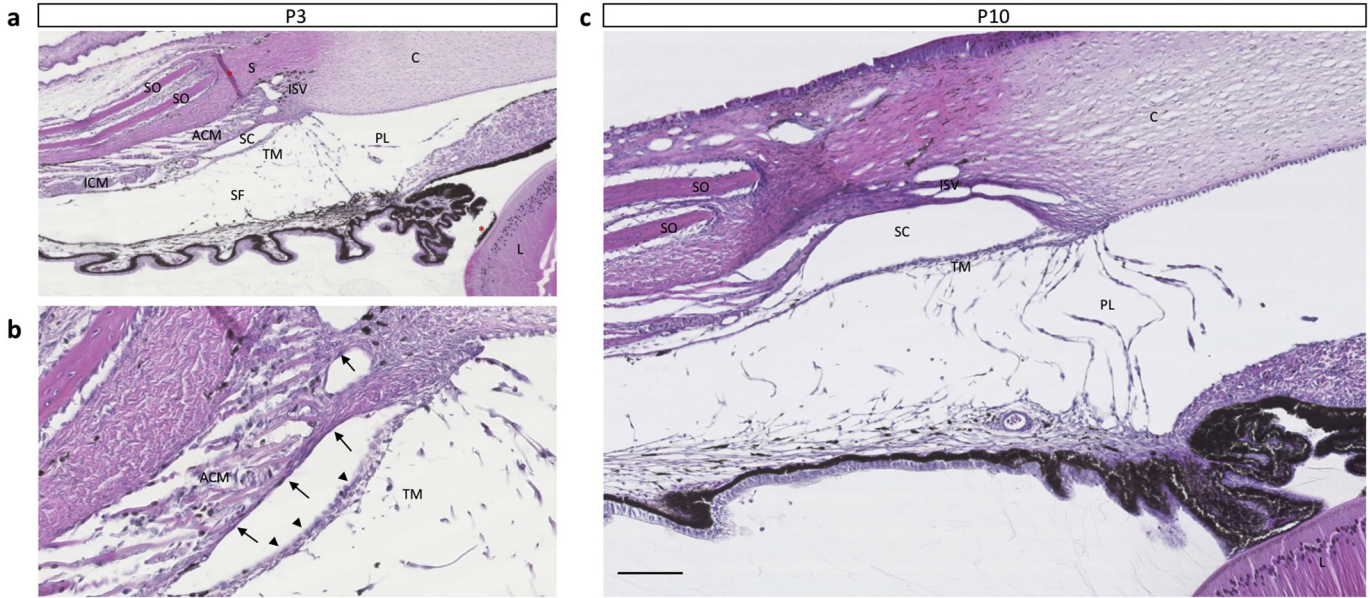
a
P3
C
S
SO
SO
ISV
ACM
SC
PL
TM
ICM
SF
L
b
ACM
TM
c
P10
C
SO
SO
ISV
SC
TM
PL
L

Figure 2

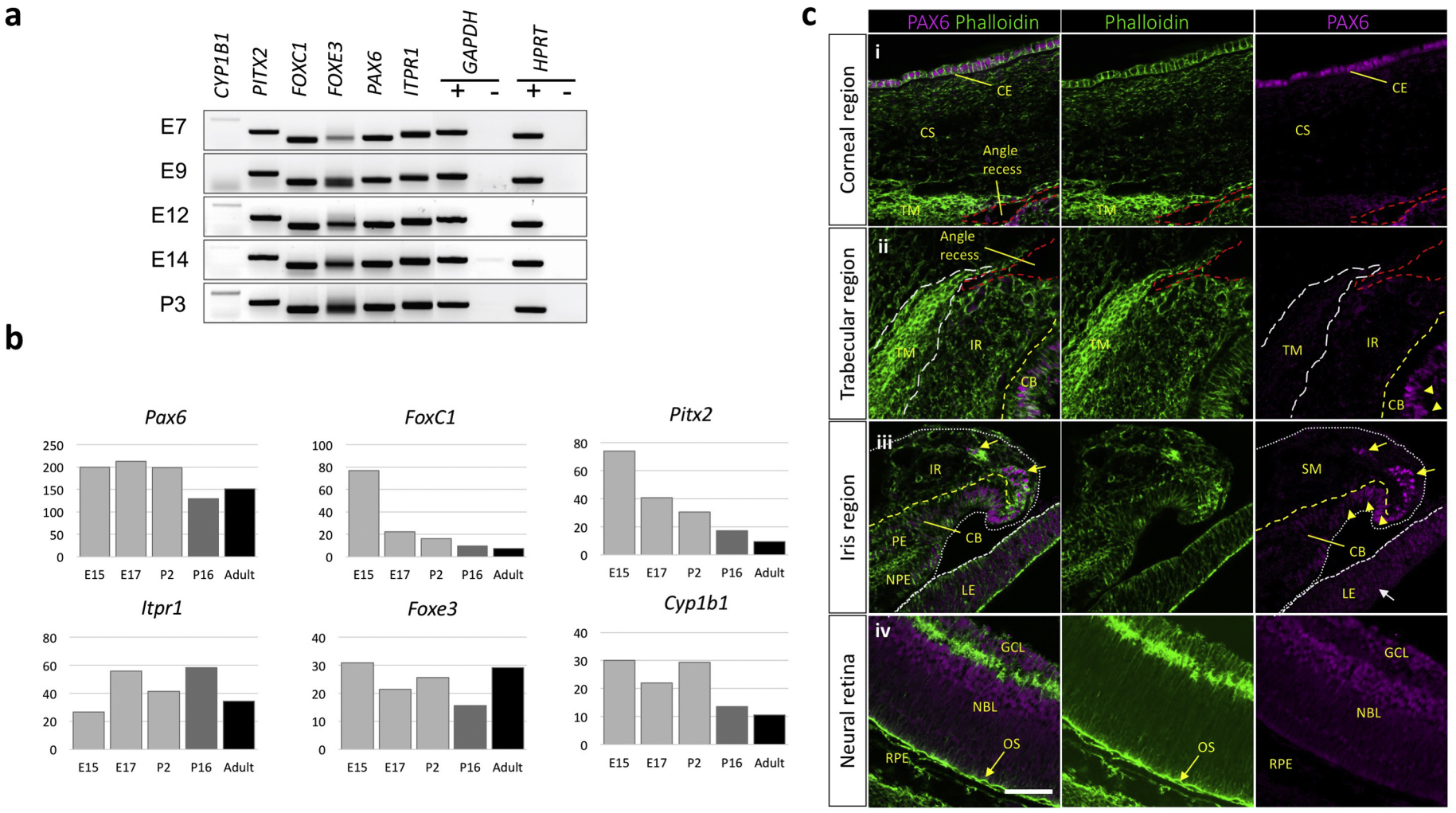
a
CYP1B1
PITX2
FOXC1
FOXE3
PAX6
ITPR1
GAPDH
HPRT
+
-
+
-
E7
E9
E12
E14
P3
b
Pax6
FoxC1
Pitx2
Itpr1
Foxe3
Cyp1b1
E15
E17
P2
P16
Adult
c
PAX6 Phalloidin
Phalloidin
PAX6
Corneal region
Trabecular region
Iris region
Neural retina
i
ii
iii
iv
CE
CS
Angle recess
TM
IR
CB
PE
NPE
LE
SM
GCL
NBL
OS
RPE

Figure 3